DAMAGE TO STRUCTURES DUE TO EXPLOSION BY DISCONTINUOUS BOUNDARY ELEMENTS

Petr P. PROCHÁZKA

Czech Technical University in Prague, Faculty of Civil Engineering, Department of Mechanics, Thákurova 7, 166 29 Prague, Czech Republic

*Corresponding author's e-mail: petrp@fsv.cvut.cz

ABSTRACT

The aim of this paper is to describe a new discrete method for the evaluation of local damage to the bearing system of underground structures. The discrete boundary element method, which serves as a numerical means for detecting local cracks, has been used in the past either as a general means for identifying sites with cracks or for assessing the possibility of bumps occurring in underground mines. Newly, this method is non-trivially extended to the combination with non-linear Navier-Stokes equations, which are solved by finite volumes used to describe the propagation of air movement that creates a subsonic pressure wave in the free space within the structure. Interaction of waves along the boundary of both phases is ensured by interfacial conditions, which correspond to the combination of both numerical means - discontinuous boundary elements and finite volumes. To maintain compatibility of both environments, discretization of both air and solid is based on hexagonal meshes. Two typical examples demonstrate the suitability of the method showing an initial (critical) state of the development of pressure waves and the condition of damage to the structures of underground parking.

1. INTRODUCTION

Today's civilized world has a very urbanized structure - a large part of the population lives in cities and underground, generally enclosed, spaces, are among the most important areas of modern towns. The utilization of underground spaces is growing rapidly. However, their structures are very vulnerable to sudden changes in load, associated with terrorist attacks, VBIED, unpredictable explosions (traffic accidents, fire, rapid economic development), etc., that can cause huge damage to structures and may have fatal consequences for human lives. Therefore, it is very important to address and anticipate the dynamic effects of explosions in enclosed spaces. The location of the explosive center is very important. It turns out that if its position is on the surface of the building or over the terrain, no follow-up wave and the interaction of the main blast wave with the secondary waves are expected. Another situation occurs when describing the time evolution in closed spaces, where wave interactions play an important role.

Propagation of blast waves in gas (air) that fill underground spaces is described by non-linear equations of conserving density, momentum and energy. The influence of gas pressure is usually given for an adiabatic state for this type of problem. The effects of explosions, i.e. initial airborne blast waves, and then interactions with secondary waves, are calculated for time changes in mass density, motion velocity and changes in internal and kinetic energy. The states of stress and deformation in the structure are also generally described by non-linear relations. Due to the relatively rapid development of the extreme load of the structural elements (plates, columns, shells, linings) after the detonation initiation, nonlinear properties predominantly involve damage and other nonlinear material changes can be considered negligible.

The issue of the effects of explosions on structures in enclosed spaces is dealt with by a number of publications, (Mitu et al., 2017; Edri et al., 2012; Li et al., 2012), for example. There are a number of publications that lead, if not directly to standards, at least to useful recommendations that come from the findings of practical knowledge, (Cioca and Moraru, 2012; Metodology manual, 2008), which are partially used in this study.

At present, the most commonly used material for underground structures is concrete, either classic, which is reinforced with steel rods or fiber-reinforced concrete. The latter is characterized by a cement matrix and unevenly distributed and randomly oriented fibers of various materials (synthetic-polypropylene, steel, glass, etc.); the fibers may also have different shapes and sizes. Thanks to these specific properties, such a composite has a higher tensile and shear strength. The abovementioned fibrous materials can be combined, (Buchana and Chenb, 2007; Luccioni and Luege, 2006). Steel fibers

serve predominantly to bridge cracks in the material, while synthetic fibers increase the ductility and deformability of the concrete. They reduce or even suppress the spalling of concrete. Appropriate application of the free hexagon method may well simulate properties of different types of fiber reinforced concrete.

In order to obtain the material properties of objects subjected to a sudden change in load, tests are carried out which, for more complex problems of the propagation of blast waves in enclosed spaces and their influence on structures are often carried out on physical and scale models, (De et al., 2010; Procházka and Trčková, 2008; Bakhtar, 1997). Compared to 1:1 or in situ models, these models make it possible to achieve very reasonable results while saving time, material and energy.

Various methods exist to describe the development of structural damage. A very efficient model using the Uzawa algorithm, (Gharizade Varnusfaderani et al., 2017; Gharizade Varnusfaderani et al., 2015; Procházka and Šejnoha, 1995), is suitable for cases where location of damage is *a priori* known. In the case that the site of the damage is not known it is advisable to use discrete elements. The basic idea was presented in 1971, (Cundall, 1971), where a continuous structure was replaced with circles or rectangles in 2D or balls or bricks in 3D. A serious problem in the method proposed by Cundal is the point contact of possible neighbors, so the definition of stress states within the particles is either inaccurate or totally excluded.

This has been overcome by solving distribution of displacements and tractions within each particle in terms of the boundary element method, in which the lowest approximation of displacements and stresses is introduced: the uniform distribution of these variables along the boundary between adjacent elements, see (Procházka, 2019; Procházka, 2014; Procházka, 2004). Similar method was proposed in (Fu et al., 2017), where time dependent kernels were used.

In some previous papers by the author of this paper, the soft contact between adjacent particles was described by the Mohr-Coulomb hypothesis. The Bureau of Mines has published several studies (Harami and Brady, 1995), where for dynamic problems it is recommended to use the Johnson and Hoek-Brown criteria, (Hoek and Brown, 1980; Girgin, 2014), instead of the previous hypothesis. The latter method offers a better approximation of Mohr's envelope, which expresses critical stresses.

The choice of initial and boundary conditions plays an important role in solving uniquely formulated problems. The goal is to get conditions that are as close to reality as possible. Such conditions are, however, very poorly defined and can be very complex. They are usually based on a large number of tests. Since the main problem in this paper focuses on solving the damage in a solid structure caused by an explosion in an enclosed space, the interfacial conditions that cause most problems are relatively well defined. In the literature, discussion of various interfacial conditions between air (fluid) and structure

can be found in (Hou et al., 2012; Subramanian, 2019; Kelliher, 2006; Naughton, 1986).

2. THE EFFECT OF AN EXPLOSION IN ENCLOSED SPACES

After detonation of explosives in various underground spaces a time-varying course of compression and tensile loads on the internal walls of the underground complex is induced. The following picture, Figure 1, illustrates such a situation in a symmetrical 2D view of a closed space. The supporting building elements can be rock, soil, tunnel lining, underground power plant lining, or parking, and possibly water pipelines. Recall that the effect of explosion in an enclosure space can also be found in building structures, such as bunkers, aircraft shelters (hangars), etc.
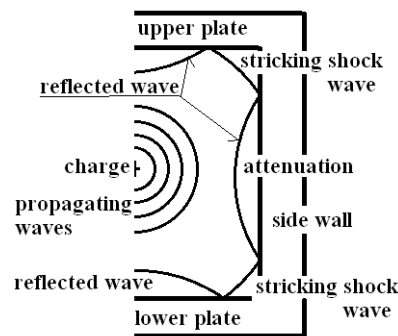

Fig. 1　Description of effect of explosion in a sample underground space.

Extreme loads caused by detonation of the explosive within a closed space can be essentially divided into several time steps (which provide more complex situations describing a combination of impact and reflective blast waves and consequently changing pressure) that can be considered decisive for the main load of the structure. In the first phase, the detonation charge causes the propagation of the blast wave in the internal airspace. After impact on the inner wall, reflection waves appear and in the next part their mutual interaction occurs. Primary and subsequent waves of this series provide very complex time curves of the total load (measured mostly by special sensors whose recording leads to the overpressure spectrum). The prediction of the first blast wave behavior is relatively easy, but the time course of the impacts of the reflected blast waves varies at different points of the internal volume and is difficult to predict.

The source of airborne impact waves can be explained on a spherical charge of a particular volume located in the air space. Detonation causes the release of the total energy of the charge, which in addition to blast waves produces gaseous chemical reaction products and so-called chamber pressure. The charge products propagate in spherical surfaces that expand. The front blast wave separates from the waste products (which are massive particles) and their effect in the air is gradually suppressed; at a distance of about 8-15 diameters of the original charges lose their significance and the waves continue only as an
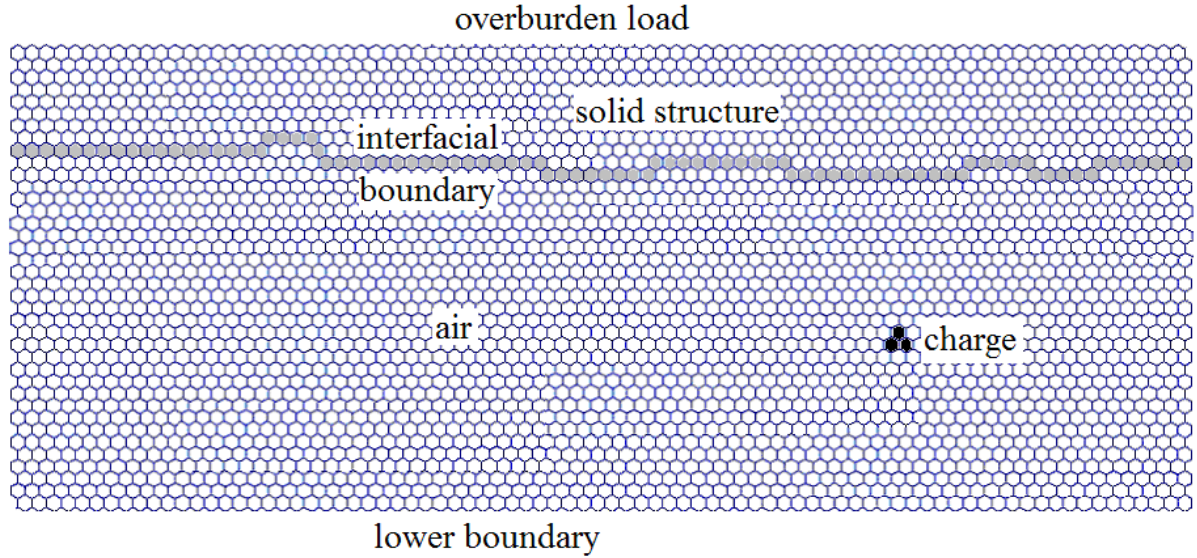
Fig. 2 The domain of the solution and the geometry of the hexagonal mesh.

original air effect. The blast wave energy also decreases considerably with increasing distance from the explosion approximately with the third root of the distance. After some time, the effect of the interaction of primary and reflected air waves is gradually lost. The predictive behavior of co-acting blast waves is not very reliable at the general point of the air domain. This is also the reason that the condition is mainly monitored in the short time after the explosion. In this timeframe, it is possible to compare the results from numerical studies and tests.

The problem can be divided into two parts, the formulation of the Landau-Lifschitz equations in the air and the response to the blast wave from the structure, formulated in terms of dynamic equilibrium. In both cases, the goal is to solve a two dimensional problems on the hexagonal mesh in the coordinate system $0x_1x_2$. The solution of both these problems is connected along the interfacial boundary between the air and the solid phase, see Figure 2. The reason why selecting a hexagonal mesh to solve a discrete problem in the structure, is obvious. This method of discretization has proved to be very suitable for monitoring the development of damage in the structure. The hexagonal mesh in final volume discretization of the air environment is chosen for the compatibility of the solid phases.

3. FINITE VOLUME METHOD ON THE HEXAGONAL MESH

In this chapter, basic ideas will be formulated regarding the problem of moving air particles as a result of an explosion within a closed space. The Euler equations, (Landau-Lifschitz, 1978), will be formulated and modified for further numerical processing.

The basic equations are formulated in the conservation form:

$$\frac{\partial \rho}{\partial t} + \frac{\partial (\rho v_1)}{\partial x} + \frac{\partial (\rho v_2)}{\partial y} = 0 \tag{1}$$

$$\frac{\partial (\rho v_1)}{\partial t} + \frac{\partial (p + \rho v_1^2)}{\partial x_1} + \frac{\partial (\rho v_1 v_2)}{\partial x_2} = 0 \tag{2}$$

$$\frac{\partial (\rho v_2)}{\partial t} + \frac{\partial (\rho v_1 v_2)}{\partial x_1} + \frac{\partial (p + \rho v_2^2)}{\partial x_2} = 0 \tag{3}$$

$$\frac{\partial e}{\partial t} + \frac{\partial [(e + p)v_1]}{\partial x_1} + \frac{\partial [(e + p)v_2]}{\partial x_2} = 0 \tag{4}$$

where t is time, and the conservative variables include the velocity vector $v \equiv \{v_1, v_2\}$, mass density of gas ρ, momentums ρv, pressure of gas $p = (\gamma - 1)\varepsilon$; potential and kinetic energies are respectively ε and $\frac{1}{2}\rho(v_1^2 + v_2^2)$, and total energy of a unit of mass of the gas is $e = \rho[\varepsilon + (v_1^2 + v_2^2)/2]$. The ratio of specific heat is γ. Equation (1) describes the conservation of mass density, the other two, (2), (3), conservation of momentums, and (4) conservation of energy.

The last four equations may be written in the matrix form as:

$$\frac{\partial A}{\partial t} + \frac{\partial B}{\partial x_1} + \frac{\partial C}{\partial x_2} = 0 \tag{5}$$

where A comprises the four conservative variables, B, and C represent the corresponding fluxes in the directions of coordinates components.

Equations (1) to (4) are strongly nonlinear. The last modification of equations (1) - (4) consists in their transcription into a quasi-linear form, the equations in which are divided into the first time and position derivatives of the vector $V = \{\rho, v_1, v_2, p\}$ of the
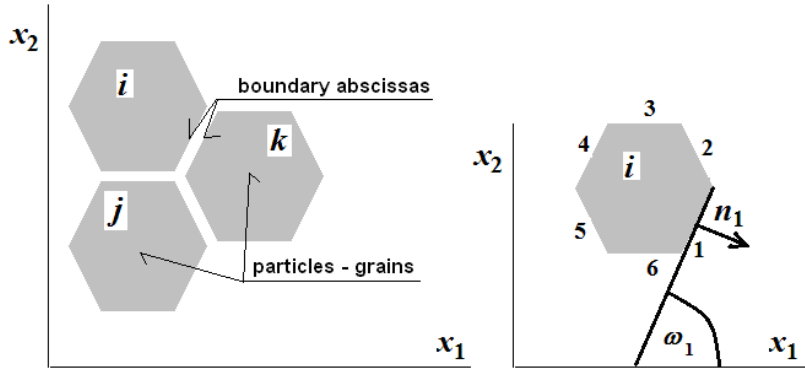
Fig. 3   Three adjacent particles and the slope of selected boundary element from the x_1- axis.

conservative variables, which is applied to the respective matrices, their members are linear:

$$\frac{\partial V}{\partial t} + A_1 \frac{\partial V}{\partial x_1} + A_2 \frac{\partial V}{\partial x_2} = 0 . \qquad (6)$$

Comparing (9) and (1) – (4), the matrices A_1 and A_2 become relatively simple:

$$A_1 = \begin{bmatrix} 0 & \rho & 0 & 0 \\ 0 & 0 & 0 & \frac{1}{\rho} \\ 0 & 0 & 0 & 0 \\ 0 & \gamma p & 0 & 0 \end{bmatrix} + Iv_1 ,$$

$$A_2 = \begin{bmatrix} 0 & 0 & \rho & 0 \\ 0 & 0 & 0 & 0 \\ 0 & 0 & 0 & \frac{1}{\rho} \\ 0 & 0 & \gamma p & 0 \end{bmatrix} + Iv_2$$

Inasmuch as the finite volume method is based on the equilibrium of the transition flows between adjacent elements, it is necessary to ensure their continuity. In Figure 3, a cutout is made from the definition area so that typical three adjacent particles can be seen that are geometrically continuous and that is also a flow.

From Figure 3 it is obvious that the boundary abscissas, marked sequentially $i = 1,...,6$, have the angle of the slope oriented with respect to the x_1 -axis and denoted as ω_i. It means that $\omega_6 = 2\pi$, for example. If the tangent (shear) direction to the abscissas is ω_i, then the outward unit normals n_i will be diverted from x_1 -axis the by an angle $\alpha_i = 3\pi / 2 + \omega_i \mod 2\pi$, $i = 1,...,6$.

Let the time be spanned from zero to the chosen time T, i.e. $t \in (0,T)$. The time interval is divided into non-overlapping subintervals $\delta t^n = [t^{(n-1)}, t^{(n)}]$, $n = 1,...,k, t^{(k)} = T$. The problem of solution of the non-linear equations (9) can be linearized in such a way that at the time $t^{(n)}$ the

components of matrices $A_1^{(t-1)}$, $A_2^{(t-1)}$ are considered as known from the previous time step $t^{(n-1)}$. Let Ω_k, $k = 1,...,m$ be a non-overlapping set of hexagons in Ω, where $\Omega \in 2D$ and the closure $\overline{\Omega}_k$, $k = 1,...,m$ completely covers Ω, i.e. $\Omega = \cup \overline{\Omega}_k \wedge \Omega_k \cap \Omega_l = \varnothing$ for $k \neq l$. The classical finite volume approximation of (6) relies on the change of the control volumes between times $t^{(n-1)}$ and $t^{(n)}$. Select arbitrary admissible k and l; $k,l \in \{1,...,m\}$, $\overline{\Omega}_k \cap \overline{\Omega}_l = S \neq \varnothing$, i.e. the last two hexagons are adjacent with the common boundary S. Next, select a time interval $\delta t = (t^{(1)}, t^{(2)}) \in (0,T)$ and choose a simpler denotation $K = \Omega_k, L = \Omega_l$. Equations (6) are then defined on $\Omega_k \times (t^{(1)}, t^{(2)}) = K \times \delta t$ and $\Omega_l \times (t^{(1)}, t^{(2)}) = L \times \delta t$, respectively. Integrating them successively over $K \times \delta t$ and then over $L \times \delta t$ yields

$$\delta t \int_K (V(x,t^{(2)}) - $$
$$- V(x,t^{(1)})) dx_1 dx_2 + A_1^{(1)} \sum_{j=1}^6 \int_{t^{(1)}}^{t^{(2)}} \int_{\partial K_j} V(x,t) n_{\partial K_j,1}(x) \, dx_1 dt +$$
$$+ A_2^{(1)} \sum_{j=1}^6 \int_{t^{(1)}}^{t^{(2)}} \int_{\partial K_j} V(x,t) n_{\partial K_j,2}(x) \, dx_2 dt = 0$$

$$(7)$$

$$\delta t \int_L (V(x,t^{(2)}) - V(x,t^{(1)})) dx_1 dx_2 +$$
$$+ A_1^{(1)} \sum_{j=1}^6 \int_{t^{(1)}}^{t^{(2)}} \int_{\partial L_j} V(x,t) n_{\partial L_j,1}(x) \, dx_1 dt + \qquad (8)$$
$$+ A_2^{(1)} \sum_{j=1}^6 \int_{t^{(1)}}^{t^{(2)}} \int_{\partial L_j} V(x,t) n_{\partial L_j,2}(x) \, dx_2 dt = 0$$

where $j = 1,...,6$, because $\partial K = \cup_{j=1}^6 \partial K_j$ and $\partial L = \cup_{j=1}^6 \partial L_j$, $n_{\partial K_j,i}$ $n_{\partial L_j,i}$ are directional cosines of the outward unit normal to ∂K_j and ∂L_j, respectively, i.e. projections of the normal to x_i, $i = 1,2$. Equations (7) and (8) can be recast as:

$$V_K^{(2)} - V_K^{(1)} + \sum_{j=1}^6 F_K^j = 0 \qquad (9)$$

$$V_L^{(2)} - V_L^{(1)} + \sum_{j=1}^{6} F_L^j = 0 \qquad (10)$$

where $V_K^{(1)}$ and $V_K^{(2)}$ are approximations of $\int_K V(x,t^{(1)}) \, dx_1 dx_2$, and $\int_K (V(x,t^{(2)}) \, dx_1 dx_2$, respectively, and, similarly, $V_L^{(1)}$ and $V_L^{(2)}$ are approximations of $\int_L V(x,t^{(1)}) \, dx_1 dx_2$, and $\int_L (V(x,t^{(2)}) \, dx_1 dx_2$, respectively. $F_K^{j,(2)}$ is an approximation of

$$F_K^j(x,t) = A_1^{(1)} \int_{t^{(1)}}^{t^{(2)}} \int_{\partial K_j} V(x,t) n_{\partial K_j,1}(x) \, dx_1 dt + \\ + A_2^{(1)} \int_{t^{(1)}}^{t^{(2)}} \int_{\partial K_j} V(x,t) n_{\partial K_j,2}(x) \, dx_2 dt \qquad (11)$$

$F_L^{j,(2)}$ is an approximation of

$$F_L^j(\mathbf{x},t) = A_1^{(1)} \int_{t^{(1)}}^{t^{(2)}} \int_{\partial K_j} V(x,t) n_{\partial L_j,1}(\mathbf{x}) \, dx_1 dt + \\ + A_2^{(1)} \int_{t^{(1)}}^{t^{(2)}} \int_{\partial L_j} V(\mathbf{x},t) n_{\partial L_j,2}(\mathbf{x}) \, dx_2 dt \qquad (12)$$

On the common interfacial boundary S of two adjacent control areas K,L, it holds at any time t,

$$n_{\partial K_j,1}(x) + n_{\partial L_k,1}(x) = 0, \\ n_{\partial L_j,2}(x) + n_{\partial L_k,2}(x) = 0, \qquad (13)$$

$x \in S = \overline{\partial K} \cap \overline{\partial L}$, $k = j + 3 \bmod 6$, hence the normal fluxes are antisymmetric along the interfaces. In the solid structure the free hexagon method with some appropriate requirements - see next chapter – will be used. Since geometric compatibility between air and solid structure is required, the nodal points are placed in the centers of the boundary abscissas of each element. This admits a simple approximation of the conservative variables that allows us to express the necessary integrals as:

$$\int_K (V(x,t^{(2)}) - V(x,t^{(1)})) dx_1 dx_2 \approx \\ \approx \frac{\text{area } K}{6} \sum_{i=1}^{6} (V(x_i,t^{(2)}) - V(x_i,t^{(1)})), x_i \in \text{center } \partial K_i, \\ \int_L (V(x,t^{(2)}) - V(x,t^{(1)})) dx_1 dx_2 \approx \\ \approx \frac{\text{area } L}{6} \sum_{i=1}^{6} (V(x_i,t^{(2)}) - V(x_i,t^{(1)})), x_i \in \text{center } \partial L_i \qquad (14)$$

Similarly,

$$F_K^j = \delta t [A_1^{(1)}(x_j)(V(x_j,t^{(2)}) n_{\partial K_j,1}(x_j) - V(x_j,t^{(2)}) n_{\partial K_j,1}(x_j)) + \\ + A_2^{(1)}(x_j)(V(x_j,t^{(2)}) n_{\partial K_j,2}(x_j) - \\ - V(x_j,t^{(2)}) n_{\partial K_j,2}(x_j))] \times \text{length } K_j \\ x_j \in \text{center } \partial K_j \qquad (15)$$

$$F_L^j = \delta t [A_1^{(1)}(x_j)(V(x_j,t^{(2)}) n_{\partial L_j,1}(x_j) - \\ - V(x_j,t^{(2)}) n_{\partial L_j,1}(x_j)) + \\ + A_2^{(1)}(x_j)(V(x_j,t^{(2)}) n_{\partial L_j,2}(x_j) - \\ - V(x_j,t^{(2)}) n_{\partial L_j,2}(x_j))] \times \text{length } K_j \\ x_j \in \text{center } \partial K_j \qquad (16)$$

The algorithm immediately follows from the above considerations: if the number of the element abscissas is n, then the number of equations to be solved at each time $t^{(n)}$ is $n \times 4$ (conservative variables) $\times 2$ (directions) $= 8n$; the same is the number of unknowns. The solution of the nonlinear equations providing the transition between successive time points is based on the predictor-corrector method. Recall that the above algorithm is based on the forward differences.

4. DISCONTINUOUS BOUNDARY ELEMENTS

The equations describing the deformation states in the structure will be formulated so that the initiation of localized damage is considered depending only on the local states of stress and strain. As a very fine mesh will be accepted, non-linear behavior inside of solid particles, such as plasticity or visco-plasticity will not be considered and all non-linear changes in the material will be described by the damage. It is worth mentioning that these properties within the particles can be extended to a much wider range of materials but as the processes in both media are very fast, the slow time-dependent material changes of the type of hereditary problems as well as plastic behaviors will be omitted in any case.

As a numerical means of localized damage caused by a rapid change of stress and deformation states in the structure due to blast waves, the discontinuous boundary elements (the free hexagon method) will be formulated and applied. This method can be included in distinct element methods, which is becoming widely accepted as an effective method of addressing engineering problems in discontinuous materials. In the case of a fine mesh of hexagons, the approximation in terms of the suggested method used the uniform distributions along the interfacial boundary of displacements and tractions. The adjacent elements are linked by springs (soft contacts), which are subject to the spring rules. The interface conditions are formulated in terms of the Lagrangian principle, in which the variables are constrained by the penalty method. The penalty parameters are spring stiffnesses. The material of springs can possess a large value to ensure the contact constrains. On the other hand, if the admissible stress is reached, the spring parameters tend to zero and naturally no energy contribution to the element boundary appears in the energy functional (the Fishera-Signorini conditions).

The hexagonal particles are studied under various contact (interfacial) conditions of the elements. Two contact conditions are adopted:

- Hoek-Brown criterion is applied instead of the standard generalized Mohr–Coulomb hypothesis (in the next, the discussion of both methods and their comparison will briefly be given),

- Elimination of tensile tractions along the contact when reaching the limit state.

The problem formulated in terms of hexagonal elements, which are not necessarily mutually

connected during the loading process (because of arising non-linearity due to the interfacial conditions) enables us to simulate the mode of propagation of cracks. The cracking of the medium can be develops so that local damage can be discovered.

For the reason of systemization, the dynamic state on one element will first be investigated. Note that the shape of individual elements is by no means restricted if their convex geometry is preserved; if the particles have the same shape, it is possible to use very fast iteration procedures because the stiffness matrix can be stored once for all in the internal memory of the computers.

4.1. DYNAMIC EQUILIBRIUM ON ONE ELEMENT.

Consider one typical hexagonal element that is described by the convex domain Ω and the boundary Γ. The boundary is composed of six abscissas $\Gamma_1,...,\Gamma_6$. The domain is equipped with a local coordinate system $0x_1x_2$. The state variables defined on $\bar{\Omega}$ are: the velocity vector $v \equiv \{v_1, v_2\}$, the mass density ρ, the fourth rank symmetric strain tensor $\varepsilon \equiv \{\varepsilon_{ij}\}_{i,j=1,2}$ and the fourth rank symmetric stress tensor $\sigma \equiv \{\sigma_{ij}\}_{i,j=1,2}$. All previous variables are position $x \equiv \{x_1, x_2\}$ and time t dependent.

The equations of elasticity in two dimensions that apply in Ω are defined by three kinematic equations, three equations of Hooke's law, and two equations of dynamic equilibrium,

$$\varepsilon_{ij}(x,t) = \frac{1}{2}\left(\frac{\partial u_i(x,t)}{\partial x_j} + \frac{\partial u_j(x,t)}{\partial x_i}\right)$$
$$\sigma_{ij}(x,t) = L_{ijkl}\varepsilon_{kl}(x,t) \tag{17}$$
$$\frac{\partial \sigma_{ij}(x,t)}{\partial x_j} = \rho\frac{\partial v_i(x,t)}{\partial t}, v_i = \frac{\partial u_i(x,t)}{\partial t}$$

where $u \equiv \{u_1, u_2\}$ is the displacement vector, L_{ijkl} are the components of the elastic material stiffness tensor of the fourth rank. The mass density ρ is assumed constant as well as the stiffness tensor, which is homogeneous and isotropic.

Integral representation of the previous equations can be recorded as

$$c_{jk}(x)u_k(\xi,t) = \int_\Gamma p_i(x,t)u_{ij}^*(x,\xi)\,dx - \int_\Gamma u_i(x,t)p_{ij}^*(x,\xi)\,dx +$$
$$+ \rho\int_\Omega \frac{\partial v_i(x,t)}{\partial t}u_{ij}^*(x,\xi)\,dx \tag{18}$$

where ξ is the point of observation, x is the integration point, $p \equiv \{p_1, p_2\}$ is the boundary tractions, c_{jk} is a diagonal matrix its values depend on the position of the point of observation. If $\xi \in \Omega - \Gamma \Rightarrow c_{jk} = \delta_{jk}$, if $\xi \in \Gamma \Rightarrow c_{jk} = \frac{1}{2}\delta_{jk}$. The quantities with asterisk are given kernels.

Denote for simplicity $b_i(x,t) = -\rho\frac{\partial v_i(x,t)}{\partial t}$.

Assuming uniform distribution of boundary quantities (displacements $u_i(x,t)$, tractions $p_i(x,t)$ and also $b_i(x,t)$) along six abscissas Γ_k, $k=1,...,6$, creating the boundary Γ, let:

$$u_i^k(t) = u_i(x_k,t), \ p_i^k(t) = p_i(x_k,t), \ b_i^k(t) = b_i(x_k,t),$$
$$x_k \in \Gamma_k, \ k=1,...,6. \tag{19}$$

where x_k, $k=1,...,6$, are centers of boundary abscissas. Positioning the points of observation ξ successively at the points ξ_k, which are the centers of boundary abscissas Γ_k of the hexagonal elements, (18) leads us to six equations of twelve dependent unknowns $u_i^k(t), p_i^k(t), i=1,2, k=1,...,6$:

$$\frac{1}{2}u_j^k(t) = p_i^k(t)\int_{\Gamma_k} u_{ij}^*(x,\xi_k)\,dx - u_i^k(t)\int_{\Gamma_k} p_{ij}^*(x,\xi_k)\,dx +$$
$$+ b_i^k(t)\int_\Omega u_{ij}^*(x,\xi_k)\,dx \tag{20}$$

or in matrix form:

$$Au(t) = Bp(t) + b(t) \tag{21}$$

As is well known, the matrix B is regular, so it can be inverted, resulting in an expression similar to finite element method:

$$Ku(t) = p(t) + Q(t), \quad K = B^{-1}A, \quad Q = B^{-1}b \tag{22}$$

Recall that the stiffness matrix K is different from that arising in applications of finite elements (here it is prevailingly non-symmetric square matrix). In many publications a certain license is introduced, namely instead of applying the above generally non-symmetric stiffness matrix the arithmetic mean of this matrix and its transposed is used. The matrices A, B, K in (24), and (25) are square matrices (12×12), u is the vector of displacement approximations, and p is the vector traction approximations; the previous two quantities are vectors (12×1), all of them are defined at nodal points (centered at the six boundary abscissas).

The matrix K can be arranged by first prioritizing the direction x_1 and then x_2. Hence, (25) will be in an index notation

$$K \equiv \begin{bmatrix} K^{11} & K^{12} \\ K^{21} & K^{22} \end{bmatrix},$$
$$\begin{Bmatrix} u^1 \\ u^2 \end{Bmatrix} \equiv \{u_1^1, u_1^2, u_1^3, ..., u_2^1, u_2^2, u_3^2, ..., u_6^2\}^T, \tag{23}$$

and similarly for p and Q.

4.2. INTERACTION OF ADJACENT ELEMENTS

Consider arbitrary selected adjacent hexagonal elements in the coordinate system $0x_1x_2$. The elements in undeformed state share a common part of element boundaries - abscissa - which belongs to both considered hexagons. Let us denote k_n the spring stiffness in the normal direction and the spring
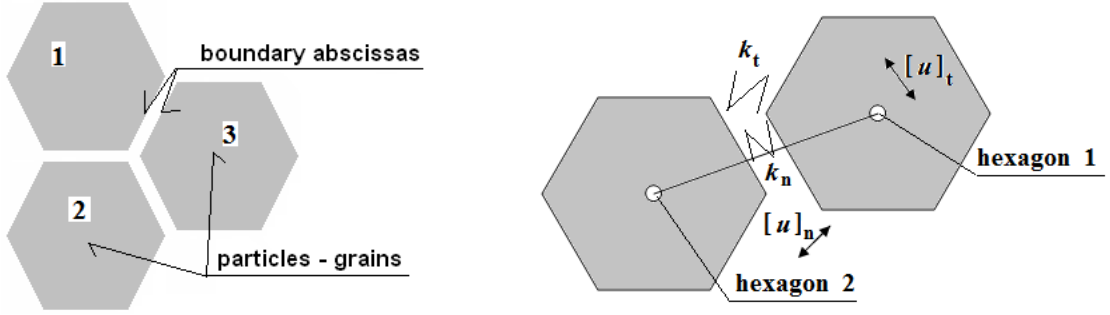
Fig. 4 Three adjacent elements (left) and denotation of contact conditions (right).

stiffness in the tangential direction as k_t on the interface. Such a case is illustrated in Figure 4.

Furthermore, after deformation, $[u]_1$ is the difference between displacement u in the x_1 direction, while the difference between displacement u in the direction x_2 is $[u]_2$, see Figure 4.

In the normal direction, adjacent elements are constrained by contact conditions, which state that no such elements can overlap each other and debonding when the tensile limit state is reached:

$$[u]_n \geq 0, \ p_n \leq p_n^+, \ \text{if} \ p_n > p_n^+ \Rightarrow p_n = 0 \qquad (24)$$

where $[u]_n$ means a jump of the displacement in the normal direction, p_n are tractions in the normal direction and p_n^+ is an admissible normal stress (traction). In the tangential (shear) direction the Mohr-Coulomb hypotheses is widely applied. A special form used in the free hexagon method is as:

$$|p_t| \leq c\kappa(p_n^+ - p_n) - p_n \tan\varphi,$$
$$\text{if} \ |p_t| > c\kappa(p_n^+ - p_n) - p_n \tan\varphi \Rightarrow p_t = p_n \tan\varphi \, \text{sgn}[u]_t \qquad (25)$$

where p_t is shear traction, $[u]_t$ is the jump in displacements in tangential direction, φ and c are material constants, κ is the Heaviside function ensuring that when the condition of $c = 0$ is met, there is a debond between adjacent particles.

Since the determination of in situ rock strength is required for successful design of underground structures, Bureau of Mines in Denver issued a series of publications, where suggestions for engineers can be found for different material properties. A recommendation that clearly follows from many tests on different materials (not only rocks) suggests that for a dynamic load, the Mohr-Coulomb hypothesis should be replaced by Hoek-Brown's criterion.

From the condition that the compression strength σ_c and the tensile strength σ^+ attain the same values for the Mohr-Coulomb and Hoek-Brown criteria it follows:

$$p_t = \left(\frac{p_n^+ - p_n}{p_n^+ - p_c}\right)^{2\beta} (c - p_c \tan\varphi)\kappa(p_n^+ - p_n). \qquad (26)$$

where κ is the Heaviside function is one for an argument greater than zero and otherwise equals zero.

The last relationship can extend the Mohr-Coulomb hypothesis and the conditions (23) and (26) can be expressed in Fischera's sense:

$$\left. \begin{array}{l} [u]_n \geq 0, \ p_n - p_n^+ \leq 0, \ [u]_n(p_n - p_n^+) = 0 \ \ \text{normal direction} \\[2mm] 0 \leq \left(\dfrac{p_n^+ - p_n}{p_n^+ - p_c}\right)^{2\beta} (c - p_c \tan\varphi)\kappa(p_n^+ - p_n) - |p_t|, \ [u]_t \geq 0, \\[3mm] \left\{\left(\dfrac{p_n^+ - p_n}{p_n^+ - p_c}\right)^{2\beta} (c - p_c \tan\varphi)\kappa(p_n^+ - p_n) - |p_t|\right\} |[u]_t| = 0 \end{array} \right\} \text{tangential direction}$$
$$(27)$$

The following picture, Figure 5, shows that the Mohr envelope according to the Hoek-Brown criterion serves much well as that by Mohr-Coulomb.

Comparing the previous condit\ions resulting from the new criterion with the conditions applicable to the Mohr-Coulomb hypothesis one concludes that it is necessary to place the Heaviside function, otherwise, in order to fulfill the realistic conditions that both tangential and normal forces are equal to zero once debonding occurs. The fraction on the right is always positive because both normal traction p_n and critical compressive force p_c are greater than admissible tensile force p_n.

Applying the "spring rule" to the neighboring elements yields, see Figure 4:

$$p_n = k_n [u]_n, \ p_t = k_t [u]_t \ \text{or} \ \begin{Bmatrix} p_n \\ p_t \end{Bmatrix} = \begin{bmatrix} k_n & 0 \\ 0 & k_t \end{bmatrix} \begin{Bmatrix} [u]_n \\ [u]_t \end{Bmatrix} \qquad (28)$$

Where k_n, k_t are normal and tangential spring stiffnesses, respectively.

The Lagrangian energy Π_1 of one particle is:

$$\Pi_1 = \frac{1}{2} a(u,u) \, dx +$$
$$+ \int_\Gamma \left\{ k_n[u]_n^2 + k_t[u]_t^2 + \left(\frac{k_n[u]_n - p_n^+}{p_c - p_n^+}\right)^{2\beta} (c - p_c \tan\varphi) |[u]_t| \, \kappa(p_n^+ - p_n) \right\} dx$$
$$(29)$$

where $a(u,u)$ is internal energy of the particle and the integral expresses the influence of boundary terms. The weak formulation (33) leads to the theory of finite elements while very weak formulation leads to boundary elements.

Note that the spring stiffnesses play the role of penalty in an expanded variational principle.
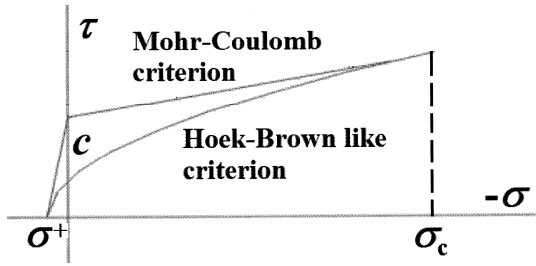
Fig. 5 Comparison of the Mohr-Coulomb hypothesis with Hoek-Brown criterion.

Fig. 6 Typical element and its neighbors.

Compared to Lagrangian multipliers that can also bind contact conditions, the solution using penalty reduces the number of unknowns. In addition, the penalty parameters are adjusted as required to meet the interfacial conditions. If k_n is large enough, the discontinuity in the normal displacements along the interface is suppressed, while, in the same time, the tangential displacements can admit possible jump. If k_t is large, the discontinuity in the tangential displacements is zero. The introduction of the Heaviside function into the formulas above will cause the tangential traction to disappear after the debond in the normal direction.

4.3. PSEUDO-STATIC LOCAL EQUILIBRIUM

Let's assume that each element is considered small enough so that a dynamic problem can be formulated by virtue of a lumped mass density centered in each element, producing the D'Alembert forces H (in horizontal direction) and V (in vertical direction). Consider further that the adjacent elements of the current element are fixed at some time instant $t^{(n)}$. The only element that can deform at the time $t^{(n)}$ is that denoted by 0 in Figure 6.

In order to ensure the equilibrium conditions in the coordinate axis directions, it will be necessary to carry out the transformation of the boundary tractions, the jumps in the displacements and the spring stiffness. For this, let's look again in Figure 4 and consider particles 1 and 3 as typical adjacent elements to study the situation at the mutual boundary.

Let the normal in the undeformed state to the boundary of particle 1, for example, be deviated from x_1 by α. Then, the transformation of tractions p from the local system to the global one can be recorded as:

$$\begin{Bmatrix} p_1 \\ p_2 \end{Bmatrix} = \begin{bmatrix} \cos\beta & -\sin\alpha \\ \sin\alpha & \cos\alpha \end{bmatrix} \begin{Bmatrix} p_n \\ p_t \end{Bmatrix} = T^T \begin{Bmatrix} p_n \\ p_t \end{Bmatrix} \tag{30}$$

where p_1 and p_2 are components of boundary tractions in x_1 and x_2 directions, respectively, T is the unitary matrix of transformation and T denotes transposition. For the jumps in displacements it similarly holds

$$\begin{Bmatrix} [u]_n \\ [u]_t \end{Bmatrix} = T \begin{Bmatrix} [u]_1 \\ [u]_2 \end{Bmatrix} \tag{31}$$
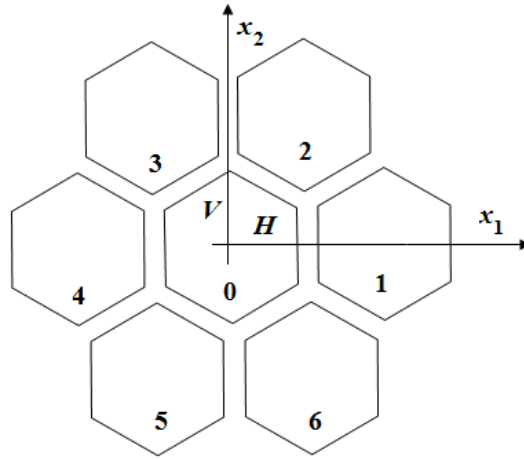
where $[u]_1$ and $[u]_2$ are projections of the jumps in displacements to the x_1- and x_2- directions, respectively. With respect to (32), (34) and (35) the following relation forces – jumps of displacements holds valid:

$$\begin{Bmatrix} p_1 \\ p_2 \end{Bmatrix} = \begin{bmatrix} k_{11} & k_{12} \\ k_{21} & k_{22} \end{bmatrix} \begin{Bmatrix} [u]_1 \\ [u]_2 \end{Bmatrix} = k \begin{Bmatrix} [u]_1 \\ [u]_2 \end{Bmatrix} \tag{32}$$

where

$$k_{11} = k_n \cos^2\alpha + k_t \sin^2\alpha, \quad k_{22} = k_t \cos^2\alpha + k_n \sin^2\alpha,$$

$$k_{12} = \frac{1}{2}(k_n - k_t)\sin 2\alpha. \tag{33}$$

Whereas (26) represents the relationship between the differences in displacements and tractions in the normal and tangential directions, (32) and (33) determine the spring coefficients in the global coordinate system $0x_1x_2$. It is worth noting that the jump in the boundary displacements on the respective borderlines is antimetric; from the equilibrium condition, the following implications apply

$$p^- + p^+ = 0 \Rightarrow k([u]^- + [u]^+) = 0 \Rightarrow [u]^- = -[u]^+ \tag{34}$$

where superscript - means "from the left", superscript + means "from the right", and k remains unchanged if one looks at the relevant boundaries in adjacent elements from the left or right.

At time t assume that all adjacent elements numbered 1 through 6 are in a deformed state fixed. It also means that boundary displacements of adjacent elements are known. Using equations (22) and (33), the D'Alembert forces H and V must be in equilibrium with the sum of all surface forces on the six boundaries. This can be expressed through a relationship

$$\begin{Bmatrix} H \\ V \end{Bmatrix} = \begin{bmatrix} K^{11} & K^{12} \\ K^{21} & K^{22} \end{bmatrix} \begin{Bmatrix} u^1 \\ u^2 \end{Bmatrix} + \sum_{j=1}^{6} k^j \begin{Bmatrix} [u]_1^j \\ [u]_2^j \end{Bmatrix},$$

$$k^j = \begin{bmatrix} k_{11}^j & k_{12}^j \\ k_{12}^j & k_{22}^j \end{bmatrix} \tag{35}$$

where k^j is the system of stiffnesses of the springs between the current element and the element $j, j = 1,...,6$, $[u]_i^j, i = 1, 2, j = 1,...,6$ are jumps in displacements in the i-direction on the boundary of the current element with the j-element. Let's note that in 12 equations there are just twelve free boundary displacements u_1^j and u_2^j in coordinate directions x_1 and x_2, respectively, and this system is always uniquely solvable. This inner iteration takes place at each time instant t.

Having once the nodal displacements known at time t, the higher order variables can easily be defined as (velocity, acceleration and inertia forces),

$$v_i(t) = \frac{\partial u_i(t)}{\partial t}, \ a_i(t) = \frac{\partial v_i(t)}{\partial t}, \ H = ma_1(t) \text{ meas } \Omega_0,$$
$$V = ma_2(t) \text{ meas } \Omega_0.$$
(36)

where meas Ω_0 is the area of the current element.

Suppose the solid structure is discretized into n elements and m internal boundaries. Moreover, Ω is the overall domain with external boundary Γ. The domains of particles is denoted as $\Omega_i, i = 1,...,n$, and the internal boundaries are $\Gamma_j, j = 1,...,m$. The Lagrangian energy Π of overall solid structure is:

$$\Pi = \frac{1}{2} E_{\text{int}} - E_{\text{ext}} + \sum_{j=1}^{m} \int_{\Gamma_j} I^j \, dx$$
(37)

where

$$E_{\text{int}} = \sum_{i=1}^{n} a^i(u, u) = \sum_{i=1}^{n} \int_{\Omega_i} (\sigma^i)^T \varepsilon^i \, dx$$

$$E_{ext} = \int_{\Gamma} \overline{p}^T u \, dx + \sum_{i=1}^{n} \int_{\Omega_i} (b^i)^T u \, dx^i$$

$$I^j = k_n^j([u]_n^j)^2 + k_t^j([u]_t^j)^2 + \left(\frac{k_n^j[u]_n^j - p_n^+}{p_c - p_n^+}\right)^{2\beta} \cdot$$
$$\cdot (c^j - p_c \tan\varphi)|[u]_t^j| \kappa(p_n^+ - p_n^j)$$

In addition, it is introduced in (39): E_{int} is the sum of internal energies over all particles, $a^i(u, u)$ is the internal energy of the $i-$th particle, E_{ext} is the energy of external forces including the sum of inertia forces, I^j are the interfacial energy density, k_n^j, k_t^j are spring stifnesses and $[u]_n^j, [u]_t^j$ are jumps in displacements on the $j-$th interfaces and the remaining quantities are considered the same on each interface, for simplicity.

5. TIME DEVELOPMENT ALGORITHM OF THE AIR - STRUCTURE SYSTEM

To be in line with the air time evolution described in section 3, let the time be spanned from zero to the selected time T, i.e. $t \in (0, T)$. The time interval is divided into non-overlapping subintervals $\delta t^n = [t^{(n-1)}, t^{(n)}], n = 1,...,k, t^{(k)} = T$. This means that every relation in the first phase of time development are observed in the current state of the air and the structure at a certain time $t^{(n)}$, depending on the conditions in the previous time step $t^{(n-1)}$. The algorithm that is proposed consists of two iteration cycles. In the first one, it is required to repeat the movement law at the nodal points of the air particles involving the interfacial conditions between the phases. Forward time differences are applied, which correspond to the procedure described in section 3, which deals with the computation of transition states between two consecutive times.

This method of back time difference also applies to the solid phase where it enters as the initial state of the so-called second inner iteration cycle. This is actually a local iteration for solving the stress and deformation states in the structure, where the development of damage is involved based on the procedure described in Section 4. Using transition conditions on the interface, i.e. the quantities received from the first iteration type in the air are set at the solid phase boundary. The individual particles are gradually processed from the discredited solid phase. The actual motion of the particles depends on adjacent elements, which are considered fixed at the time of the second cycle iteration, resolving its position relative to the immediate neighbors, and iterations will take place as long as the changes in the elements are less than the selected error. This results in the current position of the particle; the next step is to move to the next element in order. The second iteration cycle ends when greater particle movement is no longer registered.

Next, it is possible to move to next iteration of the first cycle taking place for air; there are the values of the variables from the previous iteration achieved both in the air and the interface between the two media. Then, the second iteration cycle, which applies exclusively to the structure, enters. If the time that was selected as the ending is reached, the computational process is terminated.

The equations of motion in the structure can be expressed as vector equilibrium equations in coordinate directions. If the global coordinate system is $0x_1x_2$, in each particle the equation for translational motion have to be fulfilled and can be written in the form:

$$F_i = \rho(a_i - g_i), i = 1, 2,$$
(38)

where F_i are inertia forces, which must correspond within the equilibrium to the sum of all externally applied forces on the current particle in the direction i, ρ is the mass density of the particle, $a_i \equiv \ddot{u}_i$ is the acceleration and g_i is the body force acceleration vector (e.g. loading due to gravity), which is here neglected. The translation and angular accelerations are calculated as:

$$a_i^{(n)} = \frac{1}{\delta t}(v_i^{(n)} - v_i^{(n-1)})$$
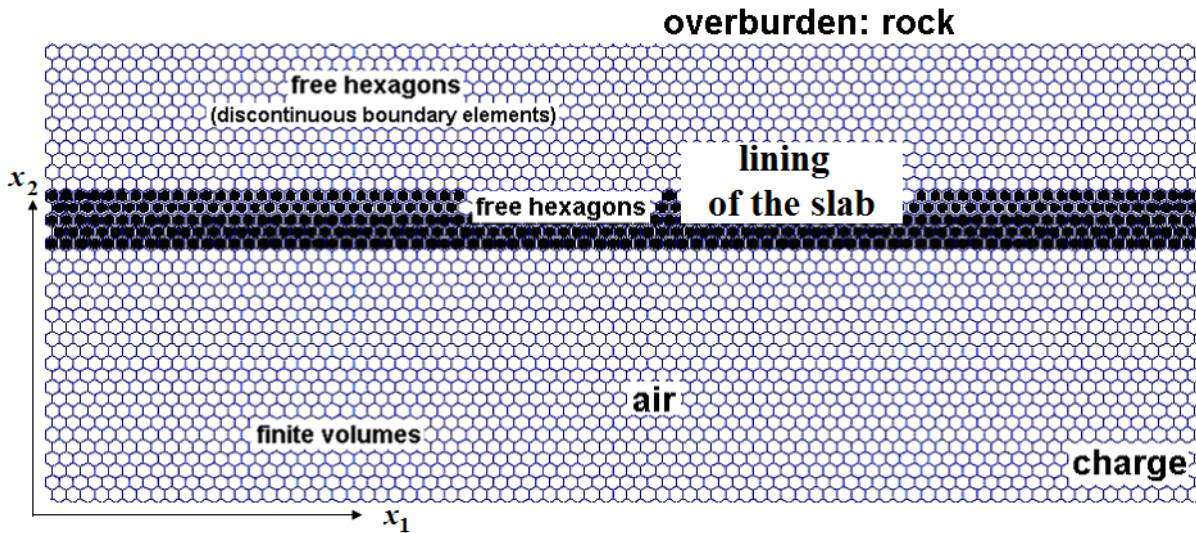(39)

Fig. 7   Geometry of the underground parking and the grains arrangement.

Inserting these velocities to the equations for motions (39) and solving it for the velocities at time (n) result in:

$$\rho[(v_i^{(n)} - v_i^{(n-1)}) / \delta t - g_i] = F_i^{(n-1)} , \qquad (40)$$

Finally, the velocities are used to update the position of the nodal point in the solid phase and also in the interfacial boundary, i.e. the displacements are attained from the relations:

$$v_i^{(n)} = (u_i^{(n)} - u_i^{(n-1)}) / \delta t , \quad u_i^{(n)} = v_i^{(n)} \delta t + u_i^{(n-1)} \qquad (41)$$

The last four equations form the initial state for internal iteration within which stress and deformation states are reached. Starting with this state, there is an internal interaction resulting in a state of structural damage. This internal iteration is performed until the all elements in the structure are in internal equilibrium with all adjacent elements. Then, one goes back to the first iterative process, that is, the situation in the time instant $t^{(n+1)}$ is to be computed based on the results from time $t^{(n)}$.

6.   EXAMPLES

Explosion in underground parking is supposed with the charge located on the bottom and at the center of vertical symmetry. The value of the radius of charge is 0.10 m, its mass $q = 50$ kg and the density of TNT $\rho_{TNT} = 1620$ kg/m³. Initial pressure of the charge is 1.3 kN/cm² and the detonation velocity is 6.94 km/sec. This information, as well as all other related to the explosion, is obtained by courteous cooperation with Austin Detonator Co, Vsetin, Czech Republic.

Material properties are introduced as: the granite rock materials remain stable inside of the particles and is given in a standard way by modules taken for linear elasticity: Young's modulus $E = 38 \times 10^9$ N/m², mass density $\rho = 7833$ kg/m³, Poisson's ratio $\nu = 0.17$, while concrete lining properties are: $E = 14 \times$ 10^9 N/m², $\rho = 2250$ kg/m³, $\nu = 0.16$, friction angle is 35^0, tensile strength is 1.26×10^6 N/m² and shear strength is 0.37×10^6 N/m². It is assumed that the rock will not suffer from damage; the displacements and stresses differences are not traversed from concrete to the rock.

In Figure 7, the geometry of the problem is seen together with the regular particles set up for the computation. Total amount of particles in our problem is 3800; from that amount 1400 define the rock, 300 covers the lining and 2100 is defined in the air. Internal diameter of each particle is 0.10 m. The height of the air space is 2.2 m, the thickness of the concrete lining is 0.5 m and the thickness of the interacting rock is 1 m. The load from overburden is 10 MPa. The time step is introduced by the value of 0.1 ms. It can be considered as a sufficient approximation.

The initial conditions are introduces for the state variables at $t = 0$:

$$\rho = \rho^0 , \quad v_1 = v_1^0 , \quad v_2 = v_2^0 , \quad p = p^0$$

where the superscript null denotes the position functions specified.

Boundary conditions:
Along the vertical external boundaries:

$$u_1 = v_1 = 0 , \quad \frac{\partial p}{\partial x_1} = 0 \quad \dots \quad \text{air}$$

$$u_1 = v_1 = 0 , \quad t_2 = 0 \quad \dots \quad \text{structure}$$
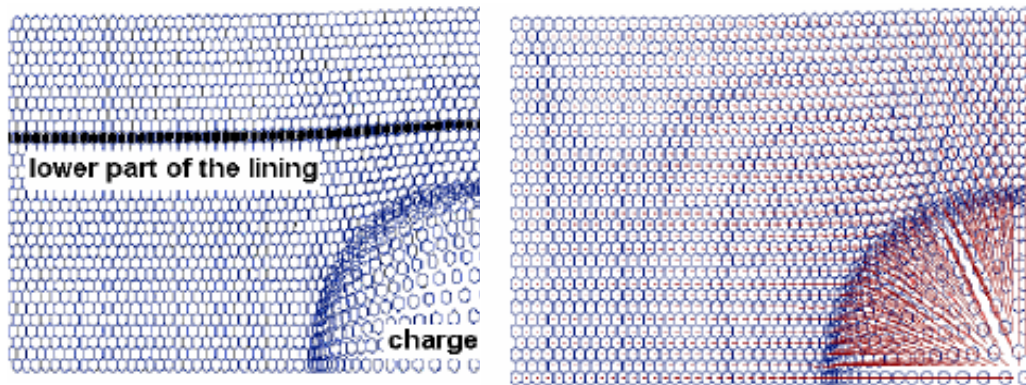
Along the bottom external boundary:

$$u_2 = v_2 = 0 , \quad \frac{\partial p}{\partial x_2} = 0 \quad \dots \quad \text{air}$$

$$u_2 = v_2 = 0 , \quad t_1 = 0 \quad \dots \quad \text{structure}$$

Along the upper external boundary: $t_2 = \sigma_0$, $t_1 = 0$

Interfacial boundary:

$$u_2^a = u_2^s , \quad v_2^a = v_2^s , \quad \mu^a \frac{\partial v_1^a}{\partial x_1} = \mu^s \frac{\partial v_1^s}{\partial x_1}$$

Fig. 8 Particle movements in 0.1 ms.

In the above notation t_1, t_2 are boundary tractions, the upper index a means air and the upper index s refers to the structure, μ is the dynamic viscosity. Because the dynamic viscosity of a gas is small compared with that of a structure, the right side of the latter equation is small, and can be considered negligible. This allows us to write

$$\frac{\partial v_1^s}{\partial x_1} = 0 \quad \text{instead.}$$

The movements in the air in a cut above the charge after 0.1 ms are seen in Figure 8, together with their vectors. Because in the longitudinal direction the situation does not change much, only the vertical cutout around the charge is shown in the following pictures.

The movements in the air in a cut above the charge after 0.1 ms are seen in Figure 8, together with their vectors. Because in the longitudinal direction the situation does not change much, only the vertical cutout around the charge is shown in the following pictures.

In Figures 9 and 10, the movement of particles is shown in 0.5 and 1.8 ms, respectively.

Figure 9 shows that the blast wave is cut into a concrete structure and causes shear damage above the source of detonation. In the pressure condition described in Figure 10 there is attenuation of the air at the location where the shear and tensile damage was indicated in the previous period of time, and now a part of concrete material is cracked and spalling occurs.

The distribution of overpressure on the lining above the charge is seen in the next picture Figure 11.

The geometry and conditions of another example are similar to the previous one, but with the same detonation parameters, the structure is higher and is supported by columns. The plate structure is therefore also thicker. The geometry of the problem is again determined by the section of the underground car park, Figure 12.
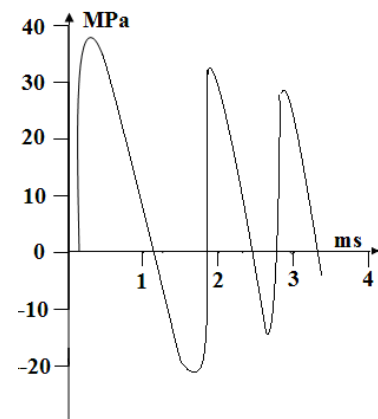
The entire domain is again composed of air and solid sub-regions; both are geometrically
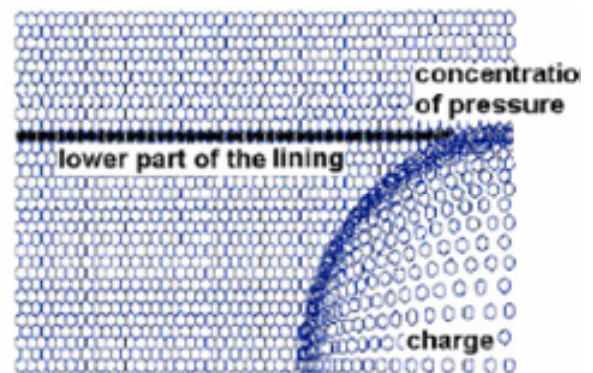
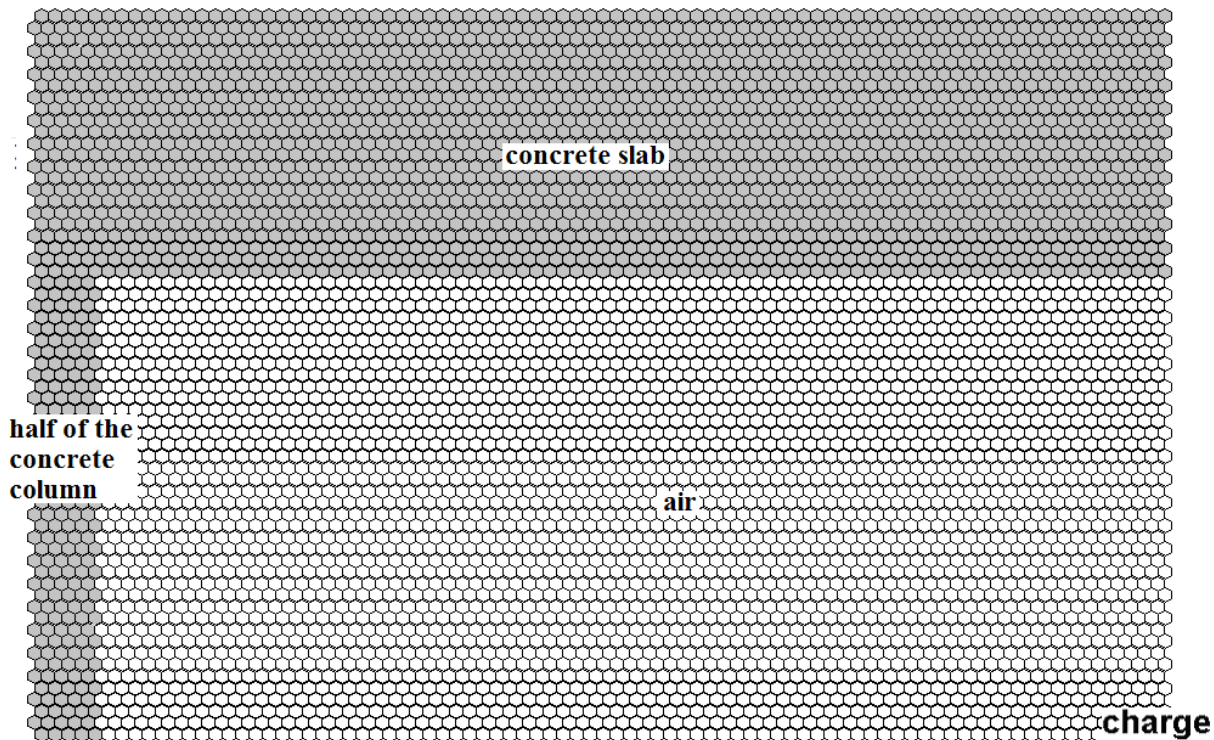**Fig. 9** Particle movements in 0.5 ms.
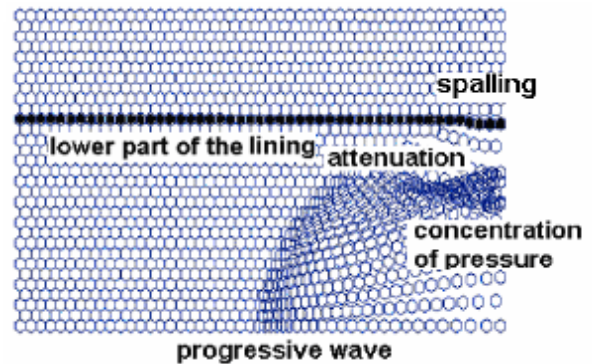
Fig. 10 Particle movements in 1.8 ms.

Fig. 11 Overpressure spectrum on the lining lower boundary above the charge.

Fig. 12 Geometry of the underground parking and the grains arrangement.

approximated by a regular hexagon mesh. The diameter of the circle of each hexagon is equal to 10 cm. The number of elements in the horizontal direction is 85 (80 is air and 5 is half of the column), vertical is 63 elements (40 approximates the area of air and 23 is in the area of the concrete slab). The total dimensions of the studied domain are: 8×3.5 m^2 is the area of air, 1 m column width, the plate has a thickness of 2 m and its half is 8 m long. In this case, it is again an underground car park that is studied in its longitudinal direction; the slab is supported by other columns whose influence is neglected due to the usual periodicity. This scheme is designed to monitor the impact of the explosion on the structure, but the purpose is not to assess the load capacity. The same detonation conditions are taken to allow comparison with the previous example.

Figure 13 shows the state at 0.8 ms when the blast wave reaches the interfacial boundary of the concrete structure and causes movement in the area of contact. The following pictures, Figures 14-16, show the evolution of overpressure over the source of the explosion in the time scale. In Figure 17, the overpressure spectrum referenced to the same location indicates that the critical values are substantially smaller than in the previous example. In this case, it is almost exclusively shear damage in the structure above the charge.

6.1. EVALUATION OF THE EXAMPLES

The dynamic behavior induced by the explosion in an enclosed air space bounded by the concrete structure of the underground car park is monitored both in the area of the propagation of the waves in the air and in the structure, where the effect of the induced

state of stress and deformation is observed. In the first case, the ceiling of the underground parking is relatively low and thus the space for the wave propagation is narrower compared to the second example. It is apparent from the pictures of the development of the wavefronts that the dumping is slow and the pressures and tensions acting on the structure alternate in quick succession. Due to the forces of pressure and tension, the structure is severely damaged, relatively large shear and tensile cracks occur, and the damage concentrates near the vertical axis of symmetry.

In the second case, the ceiling is relatively high, the lining structure is thicker and thus the situation is different compared to the previous case. Due to the large vibration space within the parking structure, the dumping is rapid, the wave force is disproportionately smaller and causes essentially only compression and tensile (not shear) damage. The pressure wave disappears relatively quickly. It should be remembered that the pressure force at the same charge mass decreases with approximately the square root of the distance.

There are some examples of the interaction of structure and shock waves in the technical and mathematical literature. For example, in the articles (Feistauer et al., 2012; Feistauer et al., 2013; Kosik, 2016), the interaction of the ear tube (similar to the tunnel) and the shock waves is monitored. Albeit these papers are based on the state of finite deformations, the procedure is considerably simpler as it assumes the interaction of air movement with the elastic solid phase. The fact that the presented article deals with the non-trivial way of damaging the lining (in our algorithm the number of iterations is possible
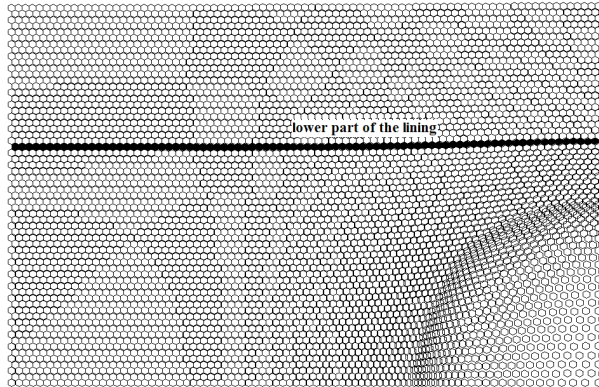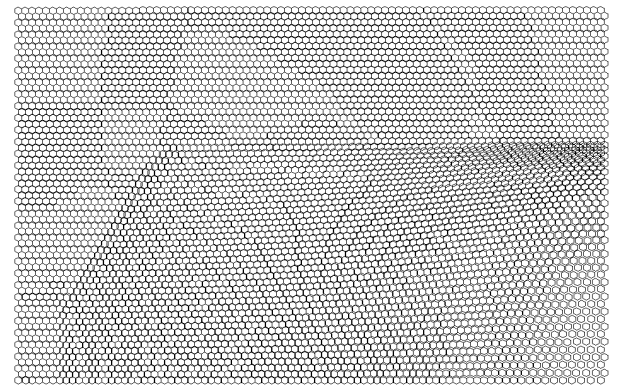
Fig. 13 Particle movements in 0.8 ms.
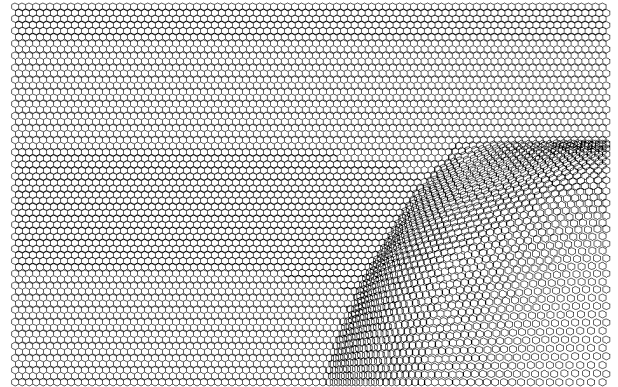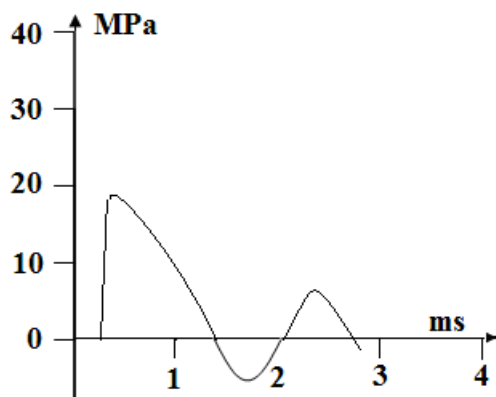

Fig. 14 Particle movements in 1.7 ms.
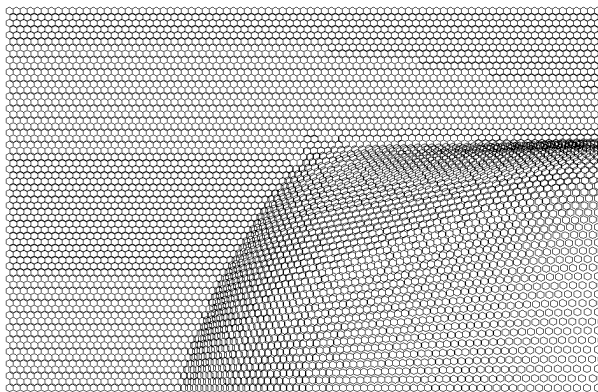
Fig. 15 Particle movements in 2.2 ms.

Fig. 16 Particle movements in 3 ms.

Fig. 17 Overpressure spectrum on the lining lower boundary above the charge.

hundreds of times compared to the procedures in the mentioned articles), the calculation procedure is much more complicated, and even the interfacial conditions have to be tuned to get the correct results.

7. CONCLUSIONS

In this paper, the numerical solution of equations for the conservation of energy, momentum and mass density is based on the finite volume method and for studying mechanical changes, namely damage to the structure; the discontinuous boundary elements - the method of free hexagons - are applied. The latter method has previously proven to be very promising for resolving a damage if its exact location is not known in advance. Since the mesh in the air should be compatible with that created in the structure, the same type of mesh is also used when finite volumes are applied. Mesh selection and other approximations are shown to be well-compatible, nodal points are concentrated in nodes located in the centers of hexagon segments (abscissas) in both media. An exception is the inertial force that is centered on the elements of the structure.

The properties of the structural material and the air are relatively well defined. On the other hand, the spring stiffness is influenced by the choice of the law of damage and a wrong choice of its coefficients can greatly affect the particle behavior of the structure. In our case, the choice of the Hoek-Brown criterion appears to be a suitable option.

In the solved examples, a regular distribution of the elements is assumed in both the air and the structure. Thus, only one stiffness matrix relating boundary tractions and displacements is provided in each element in the structure. This assumption will greatly speed up the computation, as the iterative process for detecting states in the structure for a certain time is relatively long. In addition, post-processing has been developed in the form of images that offer a better overview of the movement of particles.

ORCID: https://orcid.org/0000-0001-5604-0501

REFERENCES

Bakhtar, K.: 1997, Impact of joints and discontinuities on the blast-response of responding tunnels studied under physical modeling at 1-g. Int. J. Rock Mech. Min. Sci,, 34, 3-4, Paper No. 021.

Buchana, P.A. and Chenb, J.F.: 2007, Blast resistance of FRP composites and polymer strengthened concrete and masonry structures – A state-of-the-art review. Compos. Part B- Eng., 38, 5-6, 509–522. DOI: 10.1016/j.compositesb.2006.07.009

Cioca, I.L. and Moraru, R.I.: 2012, Explosion and/or fire risk assessment methodology: a common approach structured for underground coalmine environments. Arch. Min. Sci., 57, 1, 53–60. DOI 10.2478/v10267-012-0004-7

Cundall, P.A.: 1971, A computer model for simulation progressive large scale movements of blocky rock system. In: Symposium of the International Society of Rock Mechanics, 132-50.

De, A., Zimmie, T.F., Abdoun, T. and Tessari, A.: 2010, Physical modeling of explosive effects on tunnels. In: Fourth Int. Symp. Tunnel and Safety and Security, Frankfurt am Main, Germany, March 17-19.

Edri, I., Feldgun, V.R., Karinski, Y.S. and Yankelevsky, D.Z.: 2012, On blast pressure analysis due to a partially confined explosion: afterburning effect. Int. J. Protect. Struct., 3, 3, 311–332. DOI: 10.1260/2041-4196.3.3.311

Feistauer, M., Hasnedlová-Prokopová, J., Horáček, J., Kosik, A. and Kučera, V.: 2013, DGFEM for dynamical systems describing interaction of compressible fluid and structures. J. Comput. Appl. Math., 254, 17–30. DOI: 10.1016/j.cam.2013.03.028

Feistauer, M., Horáček, J., Kučera, V. and Prokopová, J.: 2012, On numerical solution of compressible flow in time-dependent domains. Math. Bohem., 137, 1, 1–16.

Fu, G.Y., Ma, G.-W. and Qu, X.L.: 2017, Boundary element based discontinuous deformation analysis. Int. J. Numer. Anal. Meth. Geom., 41, 7, 994–1015. DOI: 10.1002/nag.2661

Gharizade Varnusfaderani, M., Golshani, A. and Nemati, R.: 2015, Behavior of circular tunnels crossing active faults. Acta Geodyn. Geomater., 12, 4(180), 363–376. DOI: 10.13168/AGG.2015.0039

Gharizade Varnusfaderani, M., Golshani, A. and Majidian, S.: 2017, Analysis of cylindrical tunnels under combined primary near fault seismic excitation and subsequent reverse rupture. Acta Geodyn. Geomater., 14, 1(185), 5–26. DOI: 10.13168/AGG.2016.0024

Girgin, Z.C.: 2014, Modified Johnston Failure Criterion from rock mechanics to predict the ultimate strength of fiber reinforced polymer (FRP) confined columns. Polym., 6, 1, 59–75. DOI: 10.3390/polym6010059

Harami, K.Y. and Brady, B.T.: 1995, A methodology to determine in situ rock mass failure. Internal report of Bureau of Mines. Denver, CO, USA.

Hoek, E. and Brown, E.T.: 1980, Empirical strength criterion for rock masses. J. Geotech. Engng. Div. ASCE, 106, GT9, 1013–1035.

Hou, G., Wang., J. and Layton, A.: 2012, Numerical methods for fluid-structurei interaction – A review. Commun. Comput. Phys., 12, 2, 337–377. DOI: 10.4208/cicp.291210.290411s

Kelliher, J.P.: 2006, Navier-Stokes equations with Navier boundary conditions for a bounded domain in the plane. SIAM J. Math. Anal., 38, 1, 210–232.

Kosik, A.: 2016, Fluid-structure interaction. Doctoral thesis, Charles University in Prague, Faculty of Mathematics and Physics, 148 pp.

Landau, L.D. and Lifschitz, E.M.: 1985, Theoretical Physics, Hydrodynamics, Moscow: Nauka.

Li, J.C., Ma G.-W., Zhou, Y.X.: 2012, Analytical study of underground explosion-induced ground motion. Rock Mech. Rock Engng., 45, 6, 1037–1046. DOI: 10.1007/s00603-011-0200-3

Luccioni, B.M. and Luege, M.: 2006, Concrete pavement slab under blast loads. Int. J. Impact Engng., 32, 8, 1248–1266. DOI: 10.1016/j.ijimpeng.2004.09.005

Methodology Manual for the Single-Degree-of-Freedom Blast Effects Design Spreadsheets (SBEDS). US Army Corps of Engineers ® PDC TR-06-01 Rev. 1, 2008.

Mitu, M., Giurcan, V., Razus, D., Prodan, M. and Oancea, D.: 2017 Propagation indices of methane-air explosions in closed vessels. J. Loss Prevent. Process. Ind., 47, 110-119. DOI: 10.1016/j.jlp.2017.03.001

Naugton, M.J.: 1986, On numerical boundary conditions for the Navier-Stokes equations. PhD thesis, California Institute of Technology, Pasadena, USA.

Procházka, P. and Šejnoha, M.: 1995, Development of debond region of lag model. Comput. Struct., 55, 2, 249–260. DOI: 10.1016/0045-7949(94)00510-A

Procházka, P.: 2004, Application of discrete element methods to fracture mechanics of rock bursts. Engng. Fract. Mech., 71, 4-6, 601–618. DOI: 10.1016/S0013-7944(03)00029-8

Procházka, P.P. and Trčková, J.: 2008, Stress and deformation states in underground structures using coupled modeling. Acta Geodyn. Geomater., 5, 4, 361–375.

Procházka, P.P.: 2014, Rock bursts due to gas explosion in deep mines based on hexagonal and boundary elements. Adv. Engng. Softw, 72, 57–65. DOI: 10.1016/j.advengsoft.2013.06.013

Procházka, P.P.: 2019, Discontinuous boundary elements applied to the effect of explosion. Lambert Academic Publishing, Berlin, Saarbrucken.

Subramanian, R.S.: 2019, Boundary conditions in fluid mechanics. Department of Chemical and Biomolecular Engineering, Clarkson University.

http://web2.clarkson.edu/projects/subramanian/ch560/notes/ Boundary%20Conditions%20in%20Fluid%20Mechanics.pdf.